Available online at www.sciencedirect.com
SCIENCE DIRECT
Thermochimica Acta 441 (2006) 30–34
thermochimica acta
www.elsevier.com/locate/tca

Simulation of the thermal transfer during an eutectic melting of a binary solution

A. Jamil, T. Kousksou*, Y. Zeraouli, S. Gibout, J-P. Dumas

Laboratoire de Thermique Énergétique et Procédés, Avenue de l'Université, BP 1155, 64013 Pau Cedex, France

Received 20 June 2005; received in revised form 8 November 2005; accepted 10 November 2005

Abstract

The main objective of this paper is to present a model for the heat transfer in the case of the melting of saline binary solution. This model is applied to calorimetry in order to determine the kinetics of the eutectic melting. The investigated cell containing the solution is a cylinder of a few mm^3 in volume. By simulation, we could replicate the shape of the experimental thermogramms. The validation of the model permits determining some parameters which are inaccessible due to the small size of the cell, like the space-time evolution of the temperature inside the differential scanning calorimetry (DSC) sample.

Keywords: Heat transfer; Eutectic melting ; DSC; Simulation; Ammonium chloride

1. Introduction

In the previous works [1–3], we have presented some models concerning the heat transfer in the case of a phase change of binary solutions dispersed within emulsions or micro-emulsions. The different studies were related to the melting and the crystallization of the dispersed droplets. The objective was to describe the thermal transfer inside these dispersions in determining the space-time distribution of temperature and the local proportion of transformed droplets in the sample.

Sassi and Sifrini [4,5] have realized a simplified model to simulate a melting of a saline binary solution by assuming the uniformity of the temperature of the sample. The results of this model are qualitative and do not permit to find the shape of the experimental thermograms.

In this article, we present a two-dimensional model for the heat transfer in the case of the melting of a saline binary solution. This model is applied to calorimetry in order to determine the kinetics of the eutectic melting.

The model that we adopted is based on an enthalpic formulation [6]. This formulation consists in using the local liquid fraction to follow the frontal displacement of melting through a static grid. It allows to treat the phase change without taking into account explicitly the boundary condition at the solid–liquid interface.

Experiments were performed using solution of ammonium chloride NH_4Cl–H_2O at the eutectic concentration $X_e = 0.195$ and the eutectic temperature $T_e = -15.7\,^{\circ}C$.

2. Binary eutectic phase diagram

Fig. 1 is an example of a salt binary eutectic phase diagram. The liquidus line separates the salt solution phase from the ice–salt solution phase. The solidus line separates the ice–salt solution phase from the solid salt–ice phase. We note that the solidus and liquidus lines can be determined experimentally by melting and cooling samples of different compositions. These two lines cross at eutectic point (e) where can coexist the ice crystals, those of salt and the salt solution. The eutectic mixture has the lowest melting point (which is of course, the same as the freezing point) the temperature at which the eutectic mixture freezes or melts is known as the eutectic temperature T_e.

3. Study of the DSC thermograms

Apparatus PYRIS DIAMOND differential scanning calorimetry (DSC) of Perkin-Elmer will be used in this study. Fig. 2 represents the sensors or sample carriers of the apparatus.

* Corresponding author.
E-mail address: Tarik.kousksou@etud.univ-pau.fr (T. Kousksou).

0040-6031/$ – see front matter © 2005 Elsevier B.V. All rights reserved.
doi:10.1016/j.tca.2005.11.010

Nomenclature

c_p	specific heat of the eutectic solution ($J\,kg^{-1}\,K^{-1}$)
c_R	specific heat of the reference cell ($J\,kg^{-1}\,K^{-1}$)
h_1, h_2	external exchange coefficient for the cell ($W\,m^{-2}\,K^{-1}$)
L_F	latent heat of melting of the ice ($J\,kg^{-1}$)
L_D	heat of dissolution of salt in the solution ($J\,kg^{-1}$)
$T(r, z, t)$	temperature at r, z and t (°C)
T_e	melting temperature (°C)
X_e	eutectic concentration
X_g	proportion of the ice which is melted

Greek symbols

β	heating rate ($°C\,min^{-1}$)
ρ	mass density of the eutectic solution ($kg\,m^{-3}$)
ρ_g	mass density of the ice ($kg\,m^{-3}$)
λ	thermal conductivity of the eutectic solution ($W\,m^{-1}\,K^{-1}$)

The principle of DSC was outlined in Ref. [1]. The apparatus gives the energy flux dq/dt: the difference between the heat powers maintaining the plate supporting the active cell containing the eutectic solution and the plate supporting the reference cell

$$\frac{dq}{dt} = \left(\frac{dq}{dt}\right)_{\text{active cell}} - \left(\frac{dq}{dt}\right)_{\text{reference}} \tag{1}$$

As indicated in Ref. [1], the power exchanged at the reference plate is practically constant and equal to $(dq/dt)_{\text{reference}} = \beta c_R$. Where c_R is the specific heat of the reference cell and β is the heating rate. So to simplify the model we will omit the second term from the calculation of dq/dt.

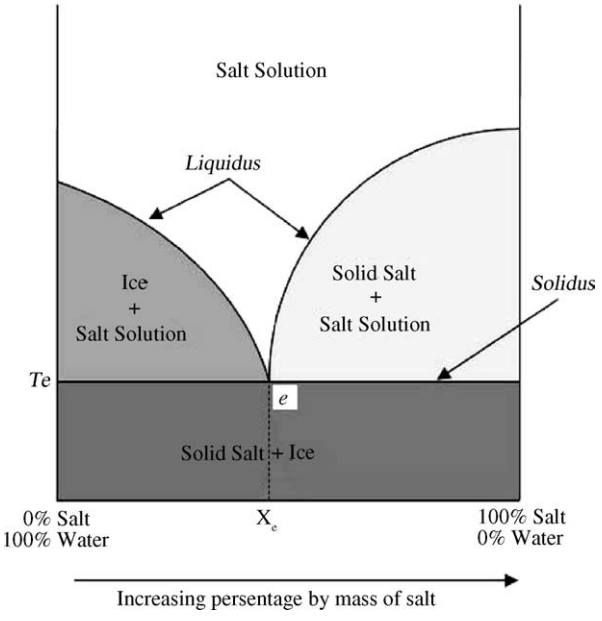

Fig. 1. Phase diagram for a binary solution.

The general pace of the thermogram obtained by calorimetry in the case of fusion of a pure substance is given by Fig. 3. We have modelled the active cell with a cylinder (Fig. 4) whose dimensions are $2R_0 = 4.25\,mm$ for the diameter and $Z_0 = 1.1\,mm$ for the height.

The model which we adopted to describe the thermal transfers during the phase shift of the studied solution is based on an enthalpic formulation proposed by Voller and his co-workers [6,7]. This formulation rests on the partition of the volume occupied by the solution into a finite number of control volumes and the handwriting the energy conservation in cylindrical coordinates:

$$\rho c_p \frac{\partial T}{\partial t} = \lambda\left(\frac{\partial^2 T}{\partial r^2} + \frac{1}{r}\frac{\partial T}{\partial r} + \frac{\partial^2 T}{\partial z^2}\right) - \rho_g A \frac{\partial X_g}{\partial t} \tag{2}$$

where ρ, c_p and λ indicate, respectively, the mass density, the specific heat and the heat conductivity of the eutectic solution. X_g indicates the proportion of the ice which is melted. The coefficient A is given by:

$$A = L_F + \left(\frac{X_e}{1 - X_e}\right) L_D \tag{3}$$

where L_F and L_D represent, respectively, the latent heat of fusion of the ice and the heat of dissolution of salt in the formed solution.

At the time of the phase change, the sample is regarded as a homogeneous material whose physical properties depend on the salt concentration and of the proportion of the ice which is melted.

To take into account the air between the solution and the cover of the cell, we consider two different heat exchange coefficient h_1 and h_2. So, the boundaries conditions are:

$$\left(\frac{\partial T}{\partial r}\right)_{r=0} = 0 \tag{4}$$

$$-\lambda\left(\frac{\partial T}{\partial r}\right)_{r=R} = h_2(T - T_{\text{plt}}) \tag{5}$$

$$-\lambda\left(\frac{\partial T}{\partial z}\right)_{z=0} = h_2(T - T_{\text{plt}}) \tag{6}$$

$$-\lambda\left(\frac{\partial T}{\partial z}\right)_{z=Z} = h_1(T - T_{\text{plt}}) \tag{7}$$

where T_{plt}, the temperature of the plates, is programmed to be linear function

$$T_{\text{plt}} = \beta t + T_0 \tag{8}$$

At $t = 0$ the initial conditions are $T(r, z, 0) = T_0$ and $X_g(r, z, 0) = 0$

Because the thermal conductivity of air is smaller than that of the metal of the cell, we consider that all the energy is transmitted to the plate by the lower boundary of the cell. So, $\frac{dq}{dt}$ is the sum of the thermal fluxes through the walls of the metallic cell

$$\frac{dq}{dt} = -\Sigma_i h_i(T_i - T_{\text{plt}})\Delta S_i \tag{9}$$

where $h_i = h_1$ or h_2.

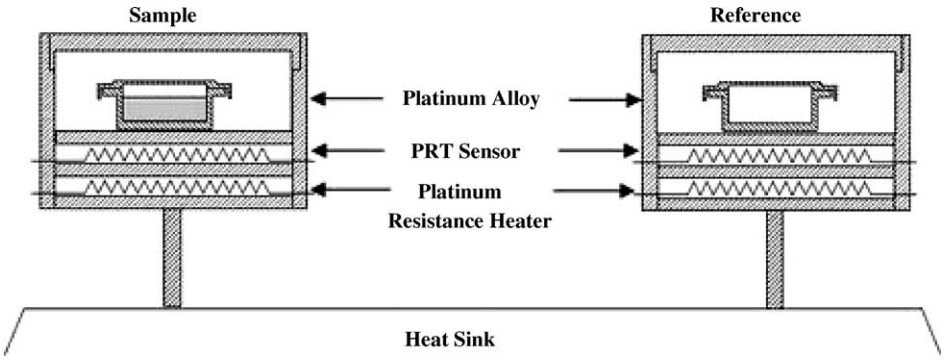

Fig. 2. Scheme of the head of the calorimeter.

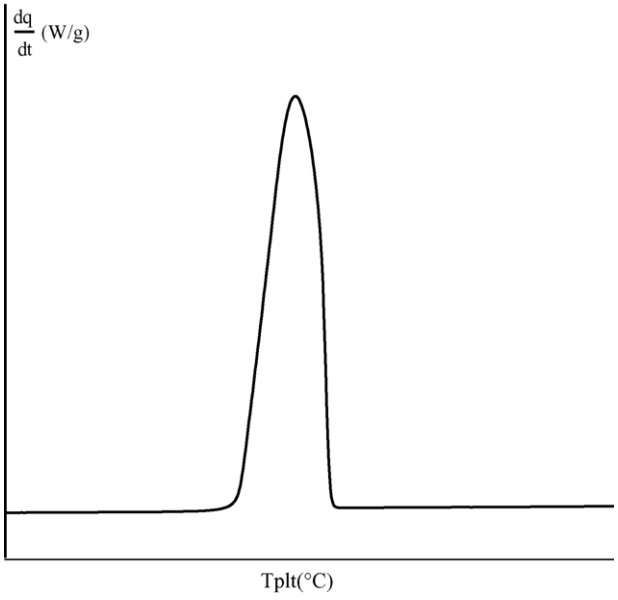

Fig. 3. Typical thermogram for the melting of the eutectic solution.

The finite-difference equations are obtained upon integrating the governing Eq. (2) over the grid-point cluster shown in Fig. 5. The resulting finite-volume scheme has the form:

$$a_P T_P = a_W T_W + a_E T_E + a_N T_N + a_S T_S + b \tag{10}$$

with

$$a_W = \frac{2\pi\lambda_w r_w \Delta z}{\Delta r} \tag{11}$$

$$a_E = \frac{2\pi\lambda_e r_e \Delta z}{\Delta r} \tag{12}$$

$$a_N = \frac{\pi\lambda_n (r_e^2 - r_w^2)}{\Delta z} \tag{13}$$

$$a_S = \frac{\pi\lambda_s (r_e^2 - r_w^2)}{\Delta z} \tag{14}$$

$$a_P = \frac{\rho_P c_p \pi (r_e^2 - r_w^2)\Delta z}{\Delta t} + a_W + a_E + a_N + a_S \tag{15}$$

$$b = \frac{\rho_P c_p \pi (r_e^2 - r_w^2)\Delta z}{\Delta t} T_P^0 - A\rho_g \pi \frac{(r_e^2 - r_w^2)\Delta z}{\Delta t} \times ((X_g)_P - (X_g)_P^0) \tag{16}$$

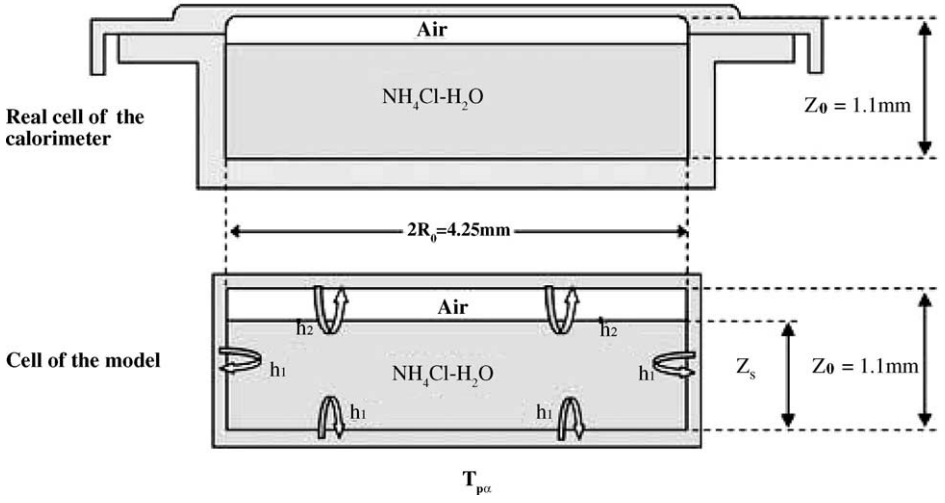

Fig. 4. Experiment cell and scheme of the model.

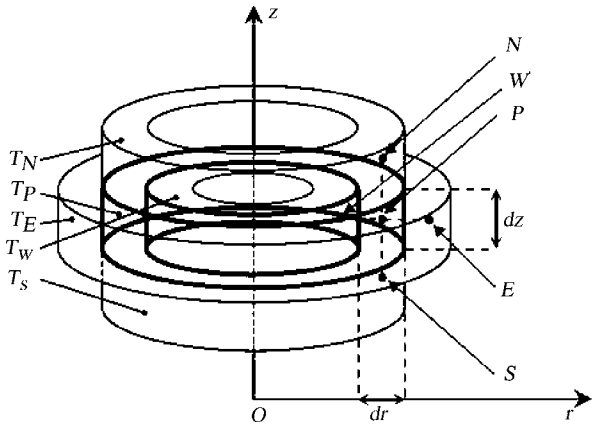

Fig. 5. Control volume.

The old (known) values of the PCM temperatures are denoted by T^0 and the new (unknown) values are denoted by T. The Eq. (10) is solved iteratively at a given time step, with a TDMA solver. The second term on the right-hand side of Eq. (2) keeps track of the latent heat evolution and its driving element is the proportion of the ice which is melted X_g. This proportion takes values of $(1 - X_e)$ in fully liquid regions, 0 in fully solid regions, and lies in the interval $[0, (1 - X_e)]$ in the vicinity of the phase front. In numerical implementation its value is determinated iteratively from the solution of the energy Eq. (10). Hence, after the ith application of the TDMA solver, Eq. (10) can be rearranged as

$$a_P T_P = a_W T_W + a_E T_E + a_N T_N + a_S T_S + \frac{\rho_P c_p \pi (r_e^2 - r_w^2)\Delta z}{\Delta t}$$

$$\times T_P^0 - A\rho_g \pi \frac{(r_e^2 - r_w^2)\Delta z}{\Delta t}((X_g)_P^i - (X_g)_P^0) \qquad (17)$$

If the phase change is occuring about the Pth node (i.e., $0 \leq (X_g)_P \leq (1 - X_e)$ and $T_P = T_e$), then the $(i + 1)$th estimate of the proportion of the ice which is melted needs to be updated so that the left-hand side of Eq. (17) is

$$a_P T_e = a_W T_W + a_E T_E + a_N T_N + a_S T_S + \frac{\rho_P c_p \pi (r_e^2 - r_w^2)\Delta z}{\Delta t}$$

$$\times T_P^0 - A\rho_g \pi \frac{(r_e^2 - r_w^2)\Delta z}{\Delta t}((X_g)_P^{i+1} - (X_g)_P^0) \qquad (18)$$

Substracting Eq. (17) from Eq. (18) yields the following update for the liquid fraction at nodes where the phase change is taking place:

$$(X_g)_P^{i+1} = (X_g)_P^i + \omega \frac{a_P \Delta t (T_P - T_e)}{A\rho_g \pi (r_e^2 - r_w^2)\Delta z} \qquad (19)$$

where ω is a relaxation parameter. This equation is applied at every node after the ith solution of the linear system Eq. (10). The iterative solution continues until convergence of the temperature at every time step.

4. Numerical and experimental results

For the numerical calculation, we have applied the procedure described in the previous section. We have used the solution of ammonium chloride NH_4Cl and water at the concentration of the eutectic $X_e = 0.195$. The diagram of phase of this solution answers the general pace of the Fig. 1.

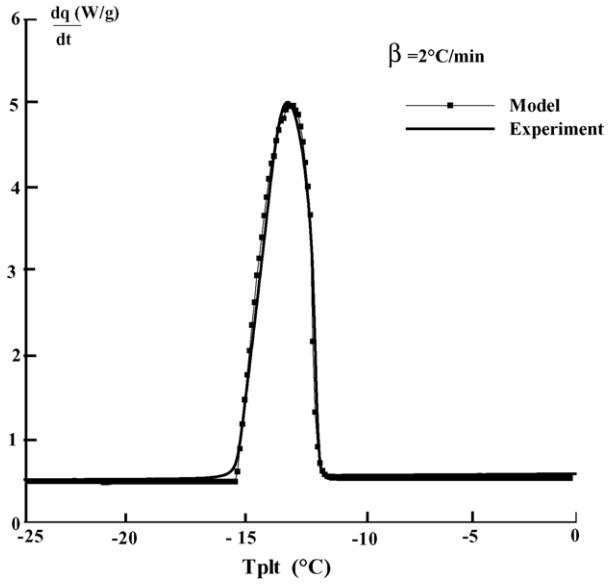

Fig. 6. Theoretical and experiment thermogram for $\beta = 2\,^\circ$C/min.

The values of physical characteristics required in the different equations have been determined experimentally or taken in the literature [8], except the coefficients of heat exchange (h_1 and h_2) that have been determined by simulation from exploratory experiments.

Fig. 6 shows an experimental thermogram for the melting of an eutectic solution ($X_e = 0.195$, $T_e = -15.7\,^\circ$C), at $2\,^\circ$C min^{-1}, compared with the calculated thermogram obtained with our model. The fit between the experimental and the calculated curves is good: the rounded form of the top of the peak is reproduced and its width is the same.

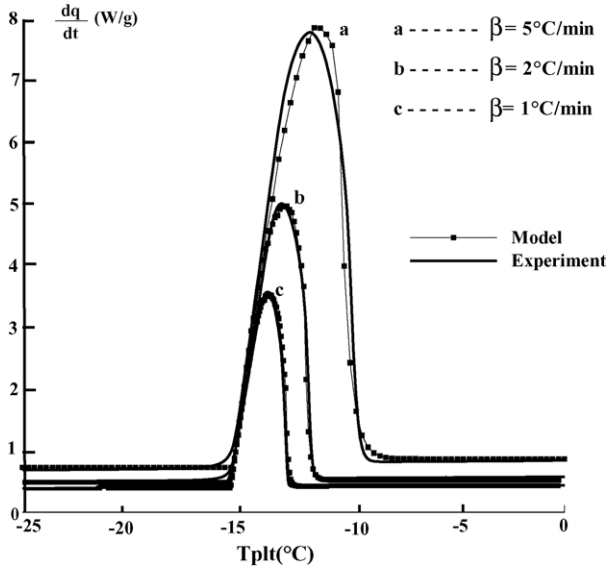

Fig. 7. Influence of the heating rate on the shape of thermograms.

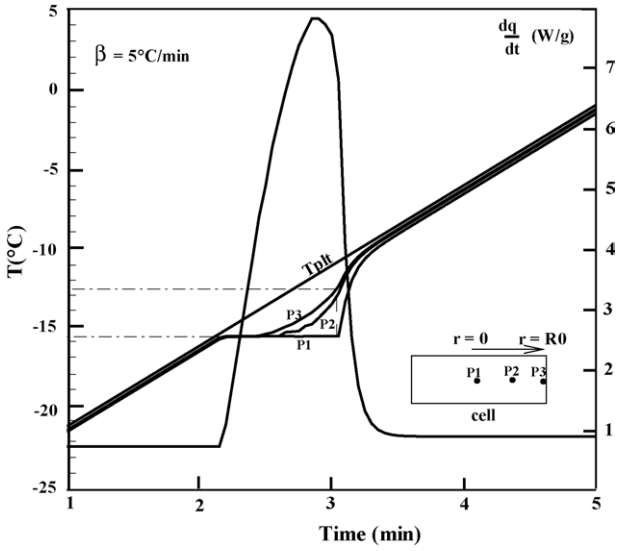

Fig. 8. Temperature versus radius for $\beta = 5\,^{\circ}$C/min.

Fig. 7 presents the thermograms obtained by the model in function of the heating rate β. These thermograms present peaks of which the height and width vary in the same direction as the heating rate. The slope of eutectic fusion remains the same in the different cases. Whereas them abscisses of the tops of the various peaks of eutectic fusion increase with β.

Figs. 8 and 9 present the temperatures T at different point of the cell and the corresponding proportion of the ice which is melted X_g versus time. Fig. 8 also includes the corresponding calculated thermogram. Important temperature differences can be observed as a function of the radius. These differences can reach 2.5 °C ($\beta = 5\,^{\circ}$C min^{-1}) at certain points. Melting begins as soon as $T = T_e$ but it is very fast near the metallic boundaries and is slower in the central region. In the central region, the melting finishes after the instant of the peak maximum. We can

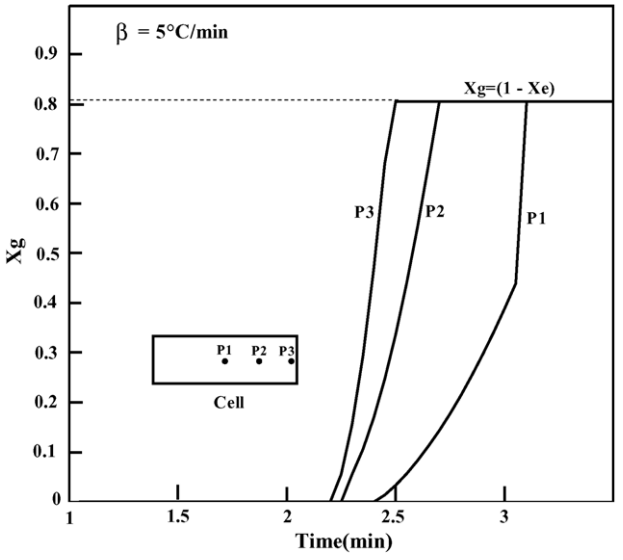

Fig. 9. X_g versus radius for $\beta = 5\,^{\circ}$C/min.

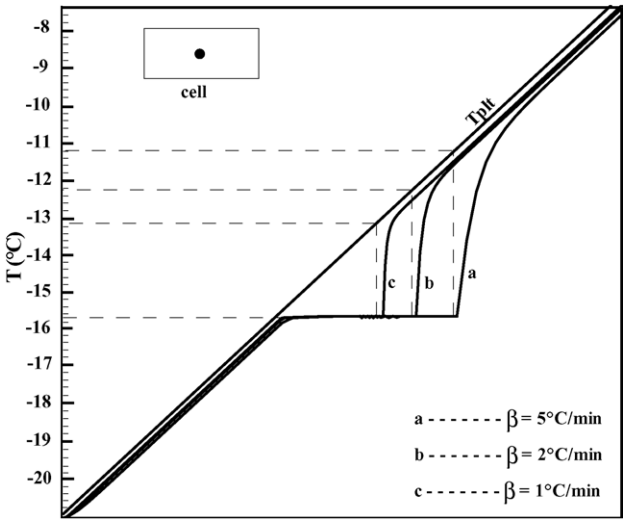

Fig. 10. Influence of ß on the temperature in the center of the sample

note that the temperature differences inside the sample due to the heat conduction within the solution.

Fig. 10 shows that the temperature difference inside cell becomes more important as the heating rate increases.

5. Conclusion

In this work, we have presented a two-dimensional model simulating the fusion (phase of the destocking) of a binary salt solution NH_4Cl–H_2O at the eutectic concentration. Despite the small dimensions of the cell, we have found important temperature gradients, responsible for the shape of the peaks. These gradients become more and more important as the heating rate increases. The application of this model to differential scanning calorimetry has permitted to understand the heat transfer nature in the investigated samples.

References

[1] J.P. Dumas, Y. Zeraouli, M. Strub, Heat transfer inside emulsions: determination of the DSC thermograms-Part 2, melting of the crystallized droplets, Thermochim. Acta 236 (1994) 239–248.
[2] J.P. Dumas, Y. Zeraouli, M. Strub, Heat transfer inside emulsions: determination of the DSC thermograms-Part 1, crystallization of the undercooled droplets, Thermochim. Acta 236 (1994) 227–237.
[3] Y. Zeraouli, A.J. Ehmimed, J.P. Dumas, Modèles de transferts thermiques lors de la fusion d'une solution binaire dispersée, Int. J. Therm. Sci. 39 (2000) 780–796.
[4] I. Sifrini, Phénomènes de cristallisations dans des solutions salines aqueuses à l'état dispersé et sous forme de gouttes, Thèse de Doctorat, Université de Pau et des Pays de l'Adour, 1983.
[5] O. Sassi, I. Siffrini, J.P. Dumas, D. Clausse, Theoretical curves in thermal analysis for the melting of binaries showing solid solution, Phase Transitions 13 (1988) 101–111.
[6] V.R. Voller, Implicit finite-difference solutions of the enthalpy formulation of stefan problems, IMA J. Numer. Anal. 5 (1985) 201–214.
[7] V. Voller, C.R. Swaminathan, General source-based method for solidification phase change, Numerical Heat Transfer, Part B 19 (1991) 175–189.
[8] J. Timmermans, The Physico-Chemical Constants of Binary Systems in Concentrated Solutions, vol. 4, New York, 1960.